Exclusive giant dipole resonance measurement on the Jacobi transition in the $^{19}F + ^{27}Al$ system

D. R. Chakrabarty,[1,*] V. M. Datar,[1] Suresh Kumar,[1] G. Mishra,[1] E. T. Mirgule,[1] A. Mitra,[1] P. C. Rout,[1] V. Nanal,[2] Deepak Pandit,[3] S. Mukhopadhyay,[3] and Srijit Bhattacharya[4]

[1]*Nuclear Physics Division, Bhabha Atomic Research Centre, Mumbai 400 085, India*

[2]*Tata Institute of Fundamental Research, Mumbai 400 005, India*

[3]*Variable Energy Cyclotron Centre, Kolkata 700 064, India*

[4]*Barasat Government College, Barasat, Kolkata 700 124, India*

(Received 31 October 2011; revised manuscript received 9 April 2012; published 27 April 2012)

Evaporation-residue-gated high-energy gamma-ray spectra were measured in the $^{19}F + ^{27}Al$ reaction at two beam energies of ∼75 and 125 MeV. The compound nuclear angular momenta populated at the higher energy should extend beyond the critical value for the Jacobi shape transition, while those at the lower energy should be mostly restricted below the critical value. A sharp low-energy (at ∼10 MeV) component has been observed in the gamma-ray strength function superimposed on a broad distribution. At the higher beam energy, the component becomes more prominent at higher angular momentum, whereas an opposite behavior is witnessed at the lower beam energy. The implication of these observations in connection with the occurrence of the Jacobi shape transition is discussed.

DOI: 10.1103/PhysRevC.85.044619 PACS number(s): 24.30.Cz, 25.70.Gh, 27.40.+z

I. INTRODUCTION

At high excitation energies, the nuclear shell effect vanishes and nuclear properties can be described as those of a charged liquid drop. In the liquid-drop regime, a rotating nucleus should have an oblate shape, with the axis of rotation coinciding with the axis of symmetry. However, at high rotational frequencies a shape transition from oblate to superdeformed triaxial (approximately prolate), similar to that in a rotating gravitational system, is expected to occur. This is known as the Jacobi shape transition. This phenomenon in rotating nuclei in the liquid-drop regime has been discussed by many authors (for example, in Refs. [1,2]). The critical angular momentum for the Jacobi transition increases with nuclear mass. In heavy nuclei (with mass number $A > 160$), the fission barrier vanishes at angular momenta below this critical value. The Jacobi transition, therefore, is amenable to study in light and medium-mass nuclei. For very neutron-rich nuclei, the fissility is expected to be lower for a given mass. The study of this shape transition may, therefore, be extended to a heavier-mass regime in future experiments with neutron-rich ion beams.

One experimental method of studying nuclear shapes at high excitation energies and angular momenta is through the measurement of the isovector giant dipole resonance (GDR) gamma decays from a compound nuclear system formed in a heavy-ion fusion reaction. The shape of the high-energy γ-ray spectrum is determined by the various nuclear shapes and their fluctuations encountered in the cooling process of a hot compound nucleus (CN).

The angular-momentum-induced shape changes from GDR measurements have been studied in light nuclei with mass number $A \sim 50$ by a number of groups. In this mass region, the Jacobi transition is expected [2] at an angular momentum ($J\hbar$) value of $\sim 28\hbar$, and the fission barrier is expected to vanish at a higher value of $J \sim 40$. The first evidence of such a transition came from the inclusive γ-ray spectra measured [3] in the $^{18}O + ^{27}Al$ reaction. The CN ^{45}Sc was formed in an excitation energy (E_X) range of 50 to 90 MeV and in the J range up to 36. In these measurements, an evolution (with beam energy) of a high-energy component at ∼25 MeV was observed in the GDR strength function, in addition to the normal one at ∼16 MeV. This was interpreted as being due to the formation of a strongly deformed shape at higher angular momenta, with the high-energy component arising due to the dipole vibration along the shortest axis. At large deformation, one expects also a low-energy component arising from the vibration along the longest axis. An evolution of a low-energy component was, however, not witnessed in this experiment. In a second experiment [4], an exclusive measurement on the GDR strength function was made in the $^{18}O + ^{28}Si$ reaction forming the CN ^{46}Ti at $E_X \sim 86$ MeV and in the J range up to ∼35. The high-energy γ-ray spectrum was measured in coincidence with characteristic discrete γ transitions in ^{42}Ca along with a condition of associated high multiplicity of low-energy γ rays. These conditions emphasised the population of high angular momenta in the CN. In this experiment a low-energy component at ∼10.8 MeV was seen in the GDR strength function in addition to two other components at ∼18 and 26 MeV. The lowest component was interpreted to be due to the vibration along the most elongated axis of the highly deformed nuclei and further shifted downward due to the Coriolis splitting. In a recent experiment [5], which was also an essentially inclusive measurement, high-energy γ rays were measured in a $^{20}Ne + ^{27}Al$ reaction populating the CN ^{47}V at $E_X \sim 108$ MeV and in the J range up to ∼38. The authors report a GDR strength function with a low-energy component at ∼10 MeV and higher energy components up to ∼27 MeV.

In the inclusive measurements [3,5], a contribution from the noncompound nuclear reactions cannot be ruled out experimentally. The exclusive measurement reported in Ref. [4] was

*drc@barc.gov.in

made in coincidence with evaporation-residue γ rays although a systematic angular momentum dependence was not studied with this experimental condition. In order to establish firmly the important observation of the Jacobi shape transition, more systematic exclusive measurements are needed to establish both its occurrence at high J and its absence at low J. For this, high-energy γ-ray spectra should be measured in coincidence with evaporation residues (for selecting the compound nuclear process) and low-energy γ-ray multiplicity (for addressing the angular momentum dependence) at various CN excitation energies.

In this paper we report the measurement of high-energy γ rays in the reaction $^{19}F + ^{27}Al$, forming the compound system ^{46}Ti, at two different energies of the ^{19}F beam. Measurements were made in coincidence with evaporation residues and a low-energy γ-ray multiplicity detector. The beam energies were chosen such that the angular momenta populated at the higher beam energy are expected to extend beyond the critical value for the Jacobi transition, while those at the lower energy should be mostly limited below this value. The present work thus addresses the issue of both occurrence of this transition at high J and its absence at low J. It should be mentioned, however, that for a light CN (as in the present case), the residue nuclei are populated in a low-J region even for a large value of J in the CN (J_{CN}). This happens because of the steeper yrast line and the relatively higher probability of alpha-particle emission in light nuclei. Thus the experimentally observed low γ-ray multiplicity events can be mapped also to higher values of J_{CN}. This makes the extraction of the shape evolution with angular momentum a little less straightforward.

II. EXPERIMENTAL DETAILS

The experiment was performed using pulsed and collimated beams of ^{19}F from the Pelletron Linac Facility (PLF), Mumbai, bombarding an Al target at two beam energies of 125 and 74.7 MeV. (Subsequently, we shall refer to the second energy as 75 MeV for brevity.) The relevant experimental information are listed in Table I. The fusion and fission cross sections (σ_{fus}, σ_{fiss}) and the critical orbital angular momentum for fusion (l_0) are from the output of a statistical model computer code mentioned later. The angular momentum populations in the CN are calculated from the product of a triangular and a Fermi distribution characterized by l_0 with a diffuseness of 2 units in l after taking the projectile and the target spins into account.

The time resolution (full width at half maximum) of the pulsed beam was typically ∼0.8 ns at the higher beam energy, for which the superconducting Linac was used as the post accelerator. At the lower beam enegy, for which only the Pelletron accelerator was used, the time resolution was typically ∼1.6 ns. For both the cases, the beam pulse separation was ∼107 ns.

TABLE I. Relevant experimental parameters. E_b is beam energy, T is target thickness, E_L is beam energy at the target center, and E_X^{CN} is mean compound nuclear excitation energy. See text for other quantities.

E_b (MeV)	T (mg/cm^2)	E_L (MeV)	E_X^{CN} (MeV)	σ_{fus} (mb)	σ_{fiss} (mb)	l_0
125	0.63	123.8	98.1	1113	82	36
74.7	0.40	73.7	68.7	1084	2	27.5

High-energy γ rays in the energy range of ∼4 to 30 MeV were detected in an array of seven close-packed BaF_2 detectors [6], each 20 cm long with a hexagonal cross section and a face-to-face distance of 9 cm. The array was placed at 125° with respect to the beam direction and at a distance of ∼50 cm from the target. This was surrounded by a 5-cm-thick and 40-cm-long annular plastic detector for active cosmic ray rejection. The setup was covered with a 10-cm-thick lead shield for reducing the cosmic γ-ray and room background. The front side had a 5-mm-thick lead sheet in order to reduce the low-energy γ rays and x rays from the target. The beam was stopped in a downstream tantalum dump placed ∼4 m from the target. The neutrons and γ rays from the dump and the upstream collimators were shielded using borated paraffin and lead, respectively. The background contributions were checked with a blank target frame and found to be negligible.

The low-energy γ-ray multiplicity was measured, in coincidence with the high-energy γ rays, with a 38-element detector array consisting of hexagonal bismuth germanate (BGO) detectors. Each BGO detector was 7.6 cm thick with a face-to-face distance of 5.6 cm. These were configured in two close-packed groups placed above and below the target. The distances of the detectors from the target were adjusted to equalize their efficiencies within ±10%. The absolute efficiency of the full array was calculated, with GEANT3 [7] simulations, to be ∼64% at 662 keV and ∼56% at 1332 keV. These values were consistent with the experimental single measurements carried out with a calibrated ^{137}Cs source and the coincidence measurements made with respect to a NaI(Tl) detector using a ^{60}Co source.

A parallel-plate avalanche counter (PPAC) of annular geometry, consisting of twelve anode sectors, was placed at a distance of ∼32 cm from the target for detecting the fusion evaporation residues. The detector was placed around the beam direction covering a forward angular range of ∼ 4°–11°. Measurement of high-energy γ-ray spectra was made both in an inclusive manner as well as in coincidence with the evaporation residues (ERs). The ER detection efficiency of the PPAC is estimated (as discussed later) to be ∼23%.

In order to assess the contribution from any oxygen impurity in the target, measurements were also made with a Ta_2O_5 target of thickness 1 mg/cm^2 deposited on a 2 mg/cm^2 Ta foil. The evaporation residues from the fusion reaction in Ta, with a maximum energy of ∼12 MeV, were stopped in the front mylar windows of the PPAC. The ER-gated spectrum from this target, therefore, originated only from oxygen.

A CAMAC-based data acquisition system was used to record the energy deposited in each BaF_2 detector and the time of arrival of the events in all the detectors (including the multiplicity array and the PPAC). The time parameters were measured with respect to the radio frequency (RF) signal synchronized with the arrival of beam bunches on the target. The neutron-gamma discrimination of the events in the BaF_2 detectors was achieved through the time-of-flight (TOF)

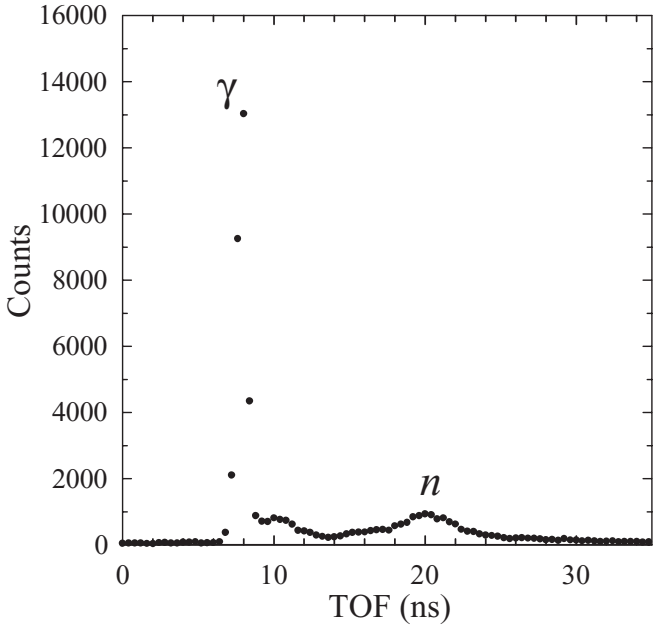

FIG. 1. TOF spectrum for one BaF_2 detector, showing prompt gamma-ray (γ) and neutron (n) induced events, at 125 MeV beam energy. Energy deposited in the detector is above 5 MeV.

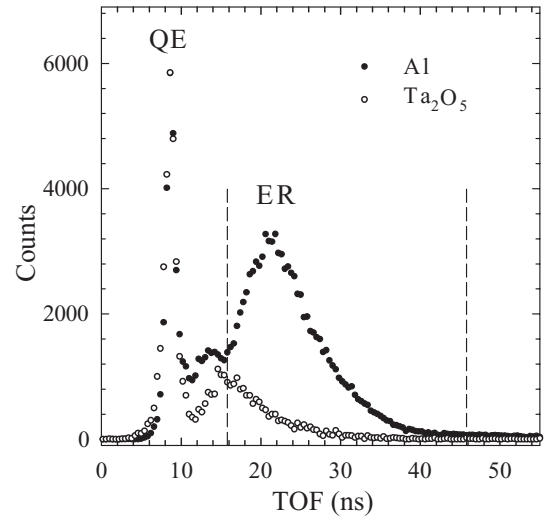

FIG. 2. TOF spectra for PPAC detector, showing the quasielastic (QE) and evaporation-residue (ER) induced events, at 125 MeV beam energy. Spectra for Al and Ta_2O_5 targets are normalized to have the same QE yields. Vertical dashed lines define the ER window used for gating.

measurement, and the pileup rejection was done by measuring the charge integrated over two time periods (~200 ns and ~2 μs) for each detector pulse and comparing the ratio with the invariant value for the "no pileup" case. The evaporation residues detected in the PPAC were identified by their TOF with respect to the RF. The data were collected for a total incident charge of 0.34 and 0.13 pmC at the high and the low beam energies, respectively, in an event-by-event mode.

The energy calibration of the BaF_2 detectors in the γ-ray energy range up to 6.13 MeV was done using ^{137}Cs, ^{60}Co, ^{241}Am-^{9}Be, and ^{238}Pu-^{13}C radioactive sources. The high voltage applied to the photomultiplier tubes attached to the detectors was so chosen as to make the energy calibration linear up to ~30 MeV. The value was ascertained from our earlier measurements with monoenergetic high-energy γ rays produced in the ^{27}Al(p,γ) and ^{11}B(p,γ) reactions as discussed in Ref. [8]. The gain variation of the detectors was periodically monitored with the radioactive sources and was taken into account in the data analysis by dividing the experimental runs into different groups. The stability was better than $\pm$0.5% among the different runs in a group.

III. EXPERIMENTAL RESULTS

Figure 1 shows an example of the TOF spectrum for the events detected in one BaF_2 detector. The prompt γ-ray induced events originating at the target are unambiguously separated from those induced by the neutrons. Figure 2 shows typical PPAC TOF spectra, gated with the γ-ray induced events in the BaF_2 detector, for the Al and Ta_2O_5 targets. The quasielastic (QE) events, induced by projectile-like fragments, and the evaporation residue (ER) events are clearly separated. Figures 3(a) and 3(b) show the fold distributions of the low-energy γ rays (from near-yrast transitions) detected in the BGO multiplicity array with and without the ER gate on the PPAC TOF. The ER gate is illustrated by the vertical dashed lines in Fig. 2. Fold (F) is defined as the number of BGO detectors simultaneously producing electronic signals in any event. The change in the F distribution with and without ER gating can be attributed to the presence of nonfusion events in the inclusive measurements.

The energy spectra of the γ rays detected in the BaF_2 detector array were generated after neutron-gamma discrimination, pileup rejection, and statistically subtracting the contribution from chance coincidences. Figures 4(a) and 4(b) show the total (F-summed) γ-ray spectra with and without ER gating. The spectral shapes for the two cases are very different at low E_γ and become similar beyond $E_\gamma \sim 15$ MeV. From a quantitative comparison of the spectra in the higher energy region (15–25 MeV), the ER detection efficiency of the PPAC can be estimated as 0.24 and 0.21 at the higher and the lower beam energies, respectively. The change in the spectral shapes, as is clearly brought out in the ratio plot, also indicates the presence of nonfusion events in the inclusive spectra. In fact, in the region of $E_\gamma \sim$ 5–12 MeV, the contribution from the nonfusion events is estimated to be as high as 75%. Therefore, only the ER-gated data were used in further analyses. The Doppler correction was finally applied to these spectra, assuming the source velocity to be that of the compound nucleus and the angle of detection to be the mean angle of the detector array. A Monte Carlo calculation reveals that the angular spread of the detector introduces negligible effect beyond this correction. For example, at the higher beam energy, it introduces a width of <0.2% and a mean energy change of 0.05%. For the lower beam energy, the effects are still less. The combination of active (plastic) and passive (lead) shields, good beam timing, and ER gating ensured that the contribution from the cosmic ray events was negligibly small.

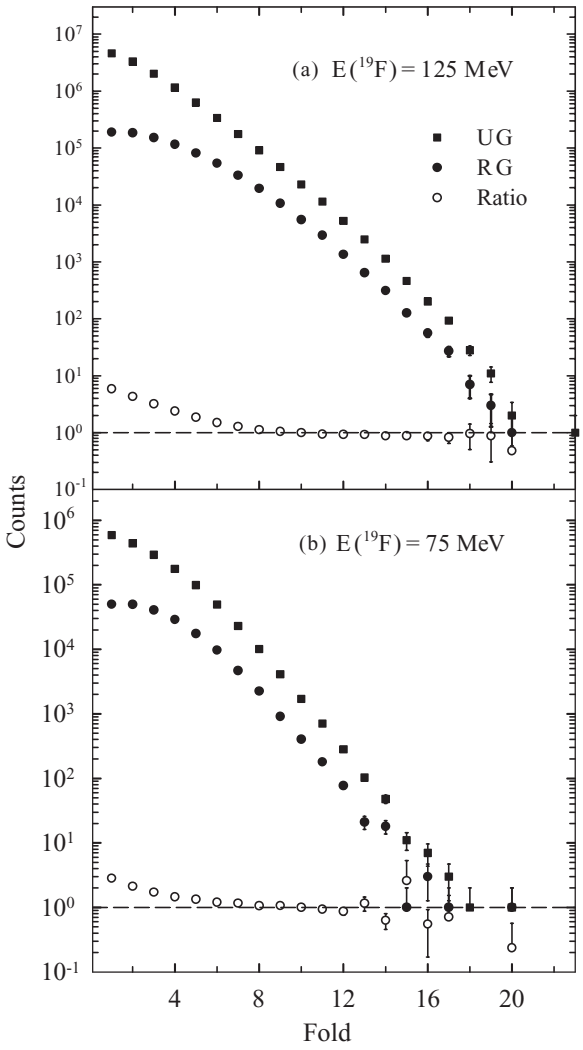

FIG. 3. F distribution of low-energy γ rays detected in the BGO array, generated with a condition of $E_\gamma \geqslant 6$ MeV in the BaF_2 detector, without (UG) and with (RG) ER gating at beam energies of (a) 125 MeV and (b) 75 MeV. Ratio (UG/RG) plots are normalized for $F \geqslant 10$. Dashed lines are drawn to visualize the departure from 1.

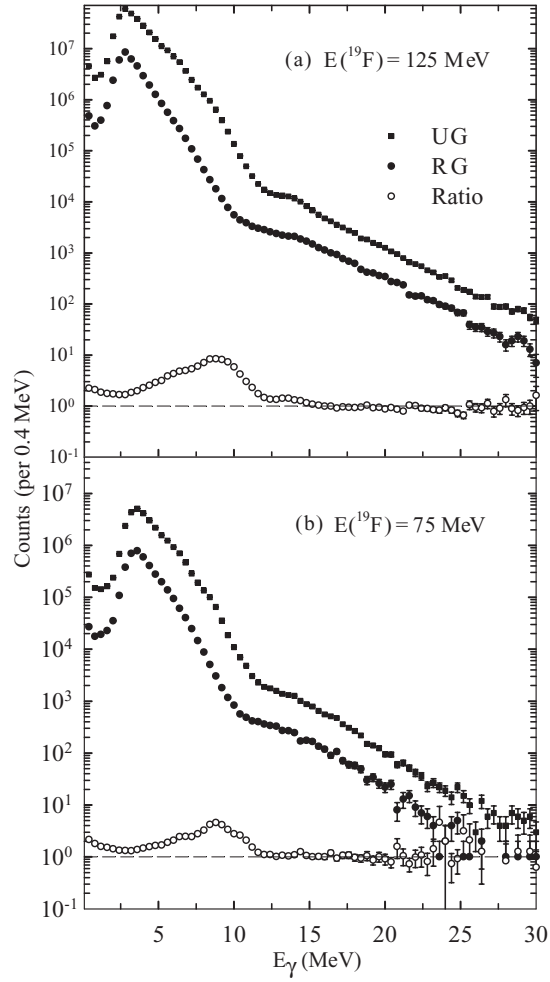

FIG. 4. F-summed γ-ray spectra (before Doppler-shift correction) without (UG) and with (RG) ER gating at beam energies of (a) 125 MeV and (b) 75 MeV. Ratio (UG/RG) plots are normalized at $E_\gamma \sim 16$ MeV. Dashed lines are drawn to visualize the departure from 1.

The exponentially falling γ-ray spectra in Fig. 4 apparently do not show any interesting features. In order to get an appreciation of the GDR strength function, these spectra were converted into the linearized "divided plots" as shown in Fig. 5. These plots were obtained in the following way. The statistical model calculations of the γ-ray spectra at the two beam energies were done using the computer code CASCADE [9]. The γ-ray strength function was assumed to have no GDR component but a constant $E1$ (electric dipole) strength, chosen arbitrarily, of 0.2 Weisskopf units (w.u.). The calculated spectra were folded with the detector response function simulated using the electron gamma shower code EGS4 [10]. The measured spectra were divided by these convoluted spectra (henceforth termed "w.u. spectra") after normalizing at ~7 MeV.

The divided plots of the F-summed spectra (Fig. 5) show different features at the two beam energies. The structure at ~10 MeV is more prominent at the higher beam energy. Although the extraction of the GDR strength function is made from a detailed statistical model analysis and not from a visual inspection of the divided plots, it is worthwhile to address whether the structures are the artifacts of division of the original spectrum by the w.u. spectrum. The latter was created with the nuclear level density (NLD) prescription of Ignatyuk *et al.* [11] with the asymptotic (liquid-drop) value of the NLD parameter $\tilde{a} = A/9$ MeV^{-1}. The yrast energies were calculated from the default option in the CASCADE code. For addressing the above question, the w.u. spectrum was changed by changing $\tilde{a}$ from $A/7.5$ to $A/10.5$ MeV^{-1} and using a shallower yrast line as prescribed in Ref. [12]. In all the cases, however, the prominence of the structure in the divided plot was evident at the higher beam energy.

The next point to address is the contributions from the target impurities (beam-induced carbon deposit or oxygen from surface oxidation) and from the nonfusion events in the target. As seen in Fig. 2, the ER peak from the main target is separated from that due to the possible oxygen impurity in

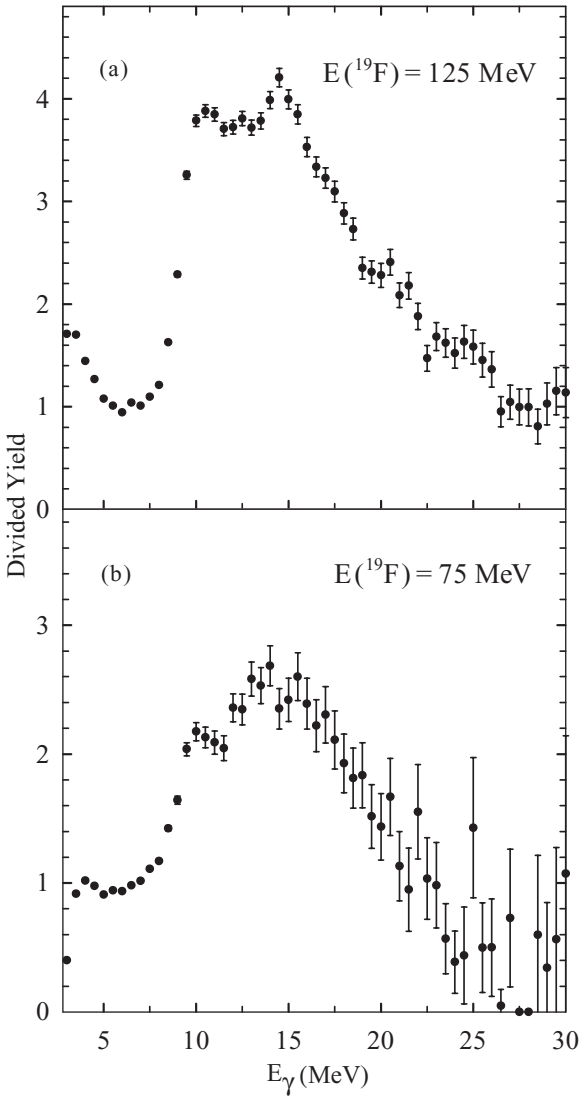

FIG. 5. ER-gated F-summed γ-ray spectra, after Doppler shift correction, presented as divided plots (see text) for beam energies (a) 125 MeV and (b) 75 MeV.

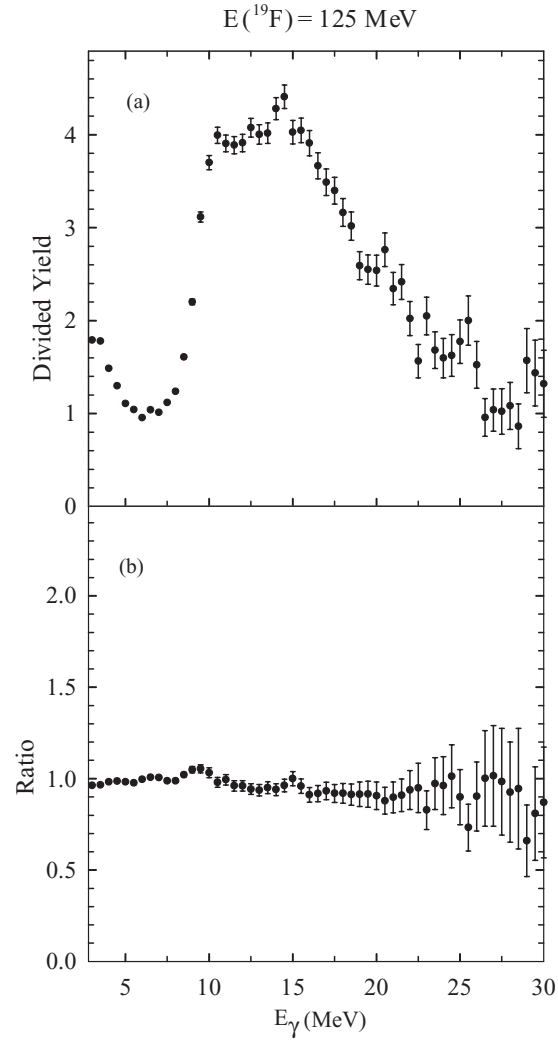

FIG. 6. (a) F-summed γ-ray spectrum with a restricted ER gate (see text) presented as a divided plot at 125 MeV beam energy. (b) Ratio of the spectra with full and restricted ER gates after normalizing at ∼15 MeV.

the target. A comparison of the spectra, generated with the ER gate shown in the figure, from the Al and Ta_2O_5 targets and an experimental estimation of oxygen content in the two targets showed that the contribution from the oxygen impurity can at best be 0.5% and, hence, is negligible. A similar conclusion can be inferred for the contribution from the lighter carbon impurity.

The nonfusion events in the target, generating high-energy γ rays, are mainly the deep inelastic and the fission events. In order to assess their contributions, Monte Carlo simulations of the TOF spectra from the evaporation residues and various binary reactions were made. For the evaporation residues, the random recoil effects due to particle evaporation leading to a spread in their kinetic energy and angle of emission were incorporated. For the binary reactions, various excitation energy and angular distributions were considered, guided by the experimental results reported in Ref. [13]. Finally, the energy loss and the multiple scattering effects in the target were included for ERs as well as the binary products. From the final energy and angle of the reaction products coming out of the target, their TOF spectra were generated from the known flight distance to the PPAC detector. The results of the simulation can be summarised as follows. The TOF spectrum for the ERs peaks at ∼22 ns, and the spectral distribution reasonably agrees with the measurement. The TOF spectra of the fission fragments and the quasielastic products peak at ∼9-14 ns, and the fractions of their yield lying in the ER gate (∼16 to 45 ns) used in the data analysis are negligible (<1%). For the deep inelastic processes with the transfer of many nucleons, the TOF of the heavier partner can infiltrate into the ER gate. For example, for a transfer of about 10 nucleons and an inelasticity of ∼50–60 MeV, the TOF lies inside the ER gate. However, considering the fraction of these events and their expected total cross sections, these contributions are also estimated to be small (<3%). We can, therefore, conclude that the measured ER-gated high-energy γ-ray spectra can be attributed to the fusion events in the Al target. Nevertheless, in order to be

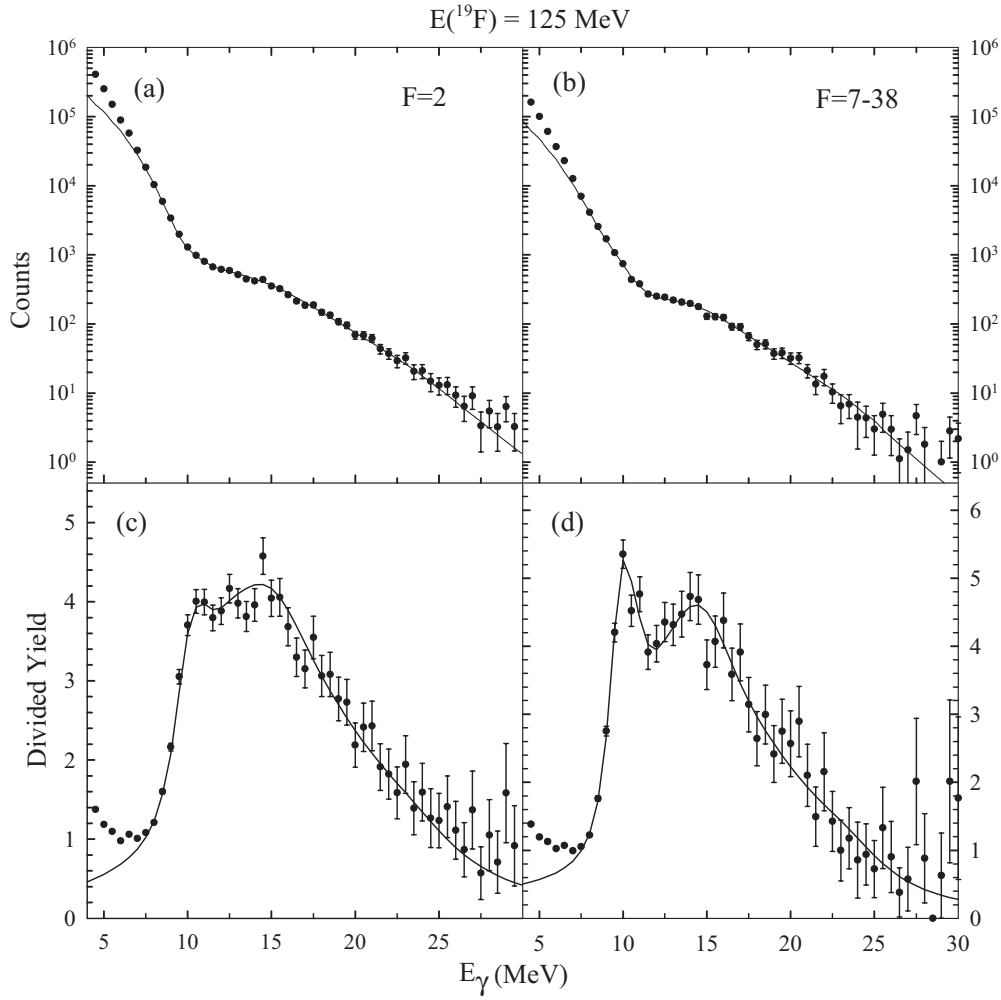

FIG. 7. ER-gated γ-ray spectra at 125 MeV beam energy for (a) $F = 2$ and (b) $F = 7$–38. The corresponding divided plots are shown in (c) and (d), respectively. Statistical model fits to the spectra are shown by the continuous lines. Fit parameters are described in the text.

more confident of this conclusion, γ-ray spectra were also generated with a restricted ER gate starting at the peak of the ER bump (Fig. 2) from the Al target. The contribution from all nonfusion events should be really insignificant under this condition. The divided plot of the inclusive spectrum thus generated is shown in Fig. 6 along with the ratio of the spectra generated with the full and the restricted ER gates. The shapes of the spectra are very similar, again indicating that the measured spectra are from the fusion events in the Al target.

IV. STATISTICAL MODEL ANALYSIS OF FOLD-GATED SPECTRA

In the earlier experiments [4,5], a component in the GDR strength function in the neighbourhood of 10 MeV has been conjectured to be a signature of the Jacobi shape transition along with the Coriolis splitting of GDR at high angular momentum. In the present work, the observation (Fig. 5) of a component at $\sim$10 MeV with its prominence diminishing at the lower beam energy is interesting in this context. This is because, as mentioned earlier, the angular momentum brought in the CN should extend well beyond the critical shape transition value only at the higher energy. It is therefore necessary to study the evolution of this component with J (via its dependence on F) at both energies, and also make a statistical model (SM) calculation of the F-gated spectra. It may be noted here that a detailed study of this type was not made in the earlier works.

Figures 7 and 8 show the F-gated γ-ray spectra and their divided plots at the two beam energies. We present data for two F windows, which are well separated and correspond to reasonably different $J_{\rm CN}$ distributions (see later discussion), considering the fact that for the present light system the mapping of F to $J_{\rm CN}$ is broad. The statistical model analysis of the spectra was done using the code CASCADE. The NLD prescription and the yrast line used in these calculations have already been mentioned in an earlier section. A few other points need to be mentioned before we present the results. First, a conventional two-component Lorentzian strength function, which can be related to a prolate or an oblate shape of the excited and rotating nuclei, could not generally fit the data. A given F window corresponds to a range of angular

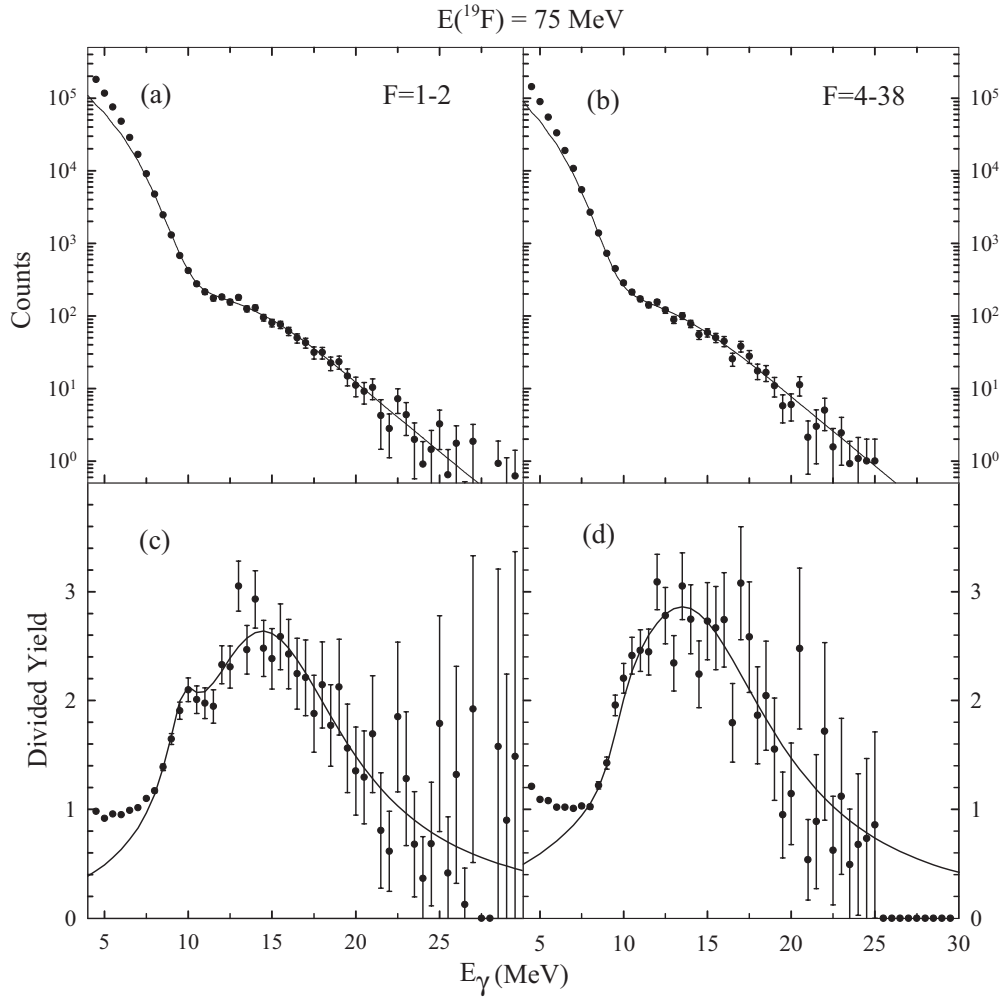

FIG. 8. The same as in Fig. 7 but for the 75 MeV beam energy and (a),(c) $F = 1$–2, (b),(d) $F = 4$–38.

momenta and, hence, various shapes involved at different steps of gamma decay. The Coriolis splitting of the GDR components is more prominent in the light nuclei than in heavier ones. The GDR built on the ground state in this mass region [14,15] is also not generally described by the one- or two-component strength functions. Considering these aspects, our approach has been to find the average GDR strength functions of a general form that is capable of describing the measured spectra. While searching for this form we have expressed this as a sum of many Lorentzians with arbitrary relative strengths. The other important point is that the statistical model analysis of the fold-gated spectra cannot be done with the conventional CASCADE code and needs a Monte Carlo approach. Moreover, one has to propose a certain dependence of the strength function on angular momentum to be incorporated at various decay steps and search for the best functional dependence. This full-fledged Monte Carlo procedure of extracting the GDR strength function is almost impractical. We have taken a somewhat simpler approach, which should be reasonable for extracting the broad features of the angular momentum dependence. From a full Monte Carlo calculation [16] with reasonable GDR parameters, the J_{CN} distribution corresponding to various fold windows (with the associated condition of the emission of γ rays in the 5 to 30 MeV range) were calculated. These distributions, shown in Fig. 9, were then used in the conventional CASCADE calculation while searching for the GDR strength function to fit the data.

The statistical model fits (after folding with the detector response function as mentioned earlier) to the F-gated data, at both the beam energies, are shown in Figs. 7 and 8 as continuous lines. At the higher beam energy, the fit shown in the figure for the lower F window has been obtained with the strength function described as a sum of five Lorentzians with the resonance energies 10.6, 13.0, 16.0, 20.0, and 24.0 MeV. The corresponding widths are 2.1, 3.8, 6.8, 7.0, and 7.5 MeV and the strengths are 9.6%, 8.8%, 56.1%, 19.72%, and 19.72% of the energy-weighted sum-rule limit (SRL), respectively. For the higher F window, again a five-component Lorentzian is used with the resonance energies 10.3, 13.0, 15.6, 20.0, and 24.0 MeV, the widths 1.5, 3.8, 6.4, 6.0, and 6.0 MeV and the strengths 16.0%, 1.2%, 71.8%, 21.9%, and 21.9% of the SRL, respectively. At the lower beam energy, the fit has been obtained for the lower F window with a two-component Lorentzian with the resonance energies 10.0 and 15.9 MeV. The corresponding widths are 1.4 and 11.5 MeV and the

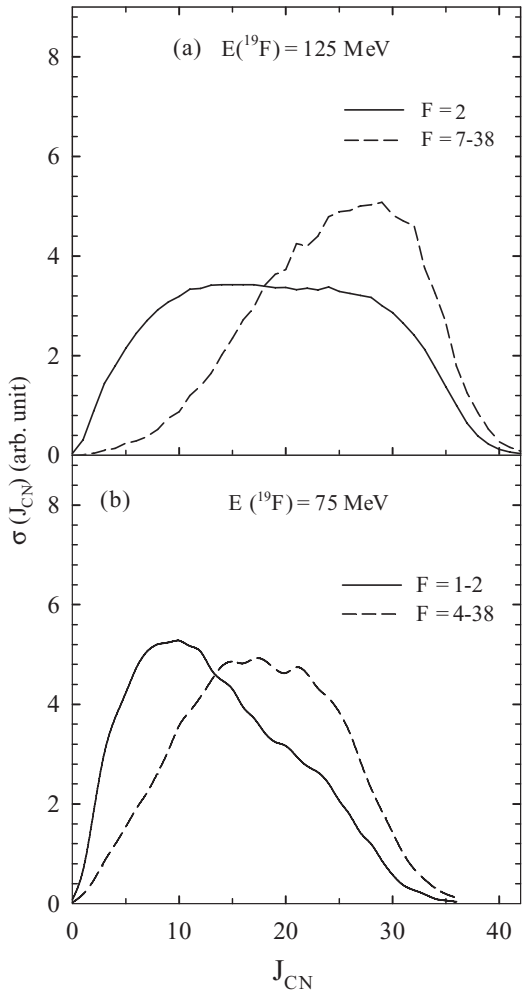

FIG. 9. Compound nuclear J distribution, corresponding to two F windows, used in the SM calculations: (a) at 125 MeV and (b) at 75 MeV beam energy. The plots are normalized to have the same integrated values.

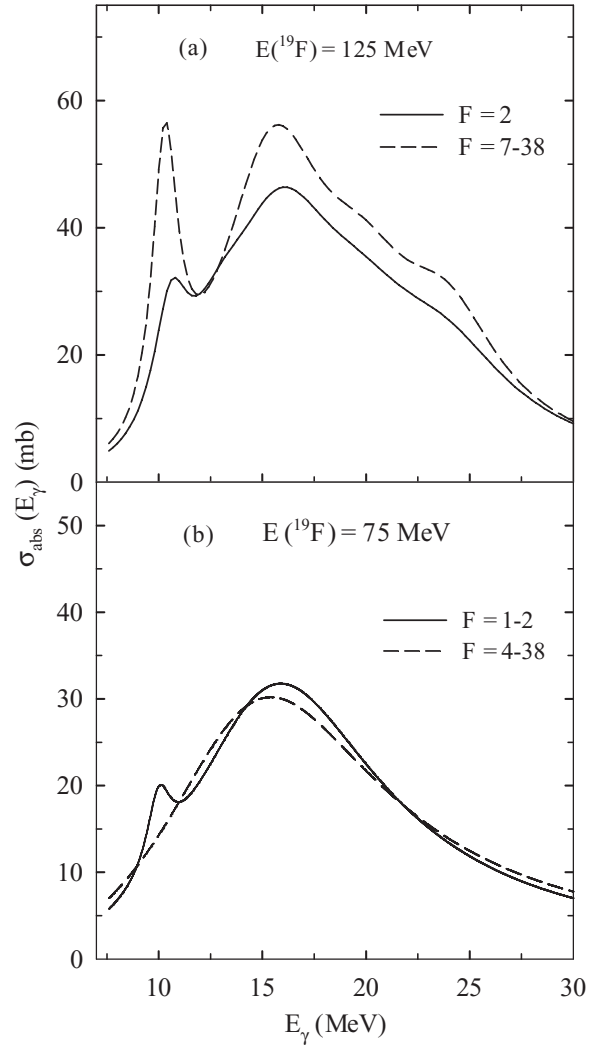

FIG. 10. Average photon absorption cross section corresponding to the fits shown in Fig. 7 at 125 MeV (a) and in Fig. 8 at 75 MeV beam energy (b).

strengths are 2.7% and 83.3% of the SRL, respectively. For the higher F window, a single-component Lorentzian with the resonance energy, width, and strength of 15.4 MeV, 13.0 MeV and 90.0% of the SRL, respectively, fits the data reasonably well.

One common feature seen in the fits of Figs. 7 and 8 is the deviation from the data below $E_\gamma \sim 7.5$ MeV. The γ rays in this energy region originate from the later part of the compound nuclear decay. One way to get the fit is by forcing the NLD to fall faster, with the decrease in the excitation energy, as compared to the prescription used in the calculation. This artificial reduction should be made only in the low excitation energy region. This prescription thus appears very arbitrary. The other possibility is the presence of enhanced electric dipole as well as electric quadrupole strengths in this γ-ray energy region. The study of the radiative strength function for low γ-ray energies is a topic of current interest [17].

The γ-ray energy dependent inverse photoabsorption cross sections corresponding to the statistical model fits are described by

$$\sigma_{abs}(E_\gamma) = \frac{4\pi e^2\hbar}{mc}\frac{NZ}{A}\sum_i \frac{S_i\Gamma_i E_\gamma^2}{\left(E_i^2 - E_\gamma^2\right)^2 + \Gamma_i^2 E_\gamma^2},$$

where E_i, Γ_i, and S_i are the energy, width, and the strength of the various components and N, Z, and A are the neutron number, proton number, and the mass number of the nucleus. The photoabsorption cross sections describing the fits shown in Figs. 7 and 8 (using N, Z, and A of the compound nucleus) are shown in Fig. 10. The experimental uncertainities in these extracted cross sections arising from the fitting procedure, which is mainly decided by the spread of the data around the fits, are not shown in these figures.

V. DISCUSSION

The average photoabsorption cross sections shown in Fig. 10 have many interesting features. At the higher beam

energy, a narrow low-energy component is seen in the cross-section profile. This becomes very prominent at the higher F window which, as illustrated in Fig. 9(a), corresponds to a J_{CN} distribution skewed to higher values. The distribution has ∼40% population above $J_{CN} = 28$, which is the expected critical value for the Jacobi transition. At the lower F value, the J_{CN} distribution is much wider and the fraction above $J_{CN} = 28$ is reduced to ∼22%. These observations imply that the low-energy component arises from an angular-momentum-driven effect. The extracted photoabsorption profile is also consistent with a higher-energy component beyond 20 MeV becoming important at the higher folds. These low- and high-energy components can be attributed (as has been done in earlier works) to the vibrations along the longest and the shortest axes of the highly deformed nuclei, encountered statistically in the cooling process of the excited compound nucleus. The present observations at the higher beam energy are therefore consistent with the occurrence of the Jacobi shape transition at high J. The range of J_{CN} populated at the lower beam energy [Fig. 9(b)] is mostly restricted below the critical value for this transition. The fraction of the population above $J_{CN} = 28$ is ∼4% and 8%, respectively, at the lower and the higher F windows shown in the figure. Thus the low-energy component in the photoabsorption profile (attributed to the Jacobi transition) should be very weak in the spectra for both the F windows. Whereas this is indeed seen to be the case for the higher F window, the presence of a low-energy component cannot be ruled out for the lower F window. However, this component is not prominent and its absence at the higher F window shows that it cannot be associated with a J-driven effect. It is possible that the component seen at the lower energy has a different origin. The broad peak in the photoabsorption cross section (on which the other components are superimposed at the higher beam energy) is seen at ∼16 MeV for both the beam energies. This should be attributed to the GDR at low values of the angular momenta. The component near 10 MeV is observed to be very narrow in the present work. In fact, it is narrower than that reported in earlier works for a component near this energy. It will be interesting to make a microscopic calculation of the GDR strength function at the temperature and angular-momentum ranges of the present work to address this issue.

The present observations imply that the Jacobi shape transition takes place at a high angular momentum. The present findings are consistent with this critical angular momentum being in the region of $28\hbar$, as predicted by theoretical calculations although a very precise experimental value for this has not been deduced. If the F-to-J_{CN} mapping were narrower, it would be possible to extract a better defined value from the analysis of the measured γ-ray spectra in finer steps of F. The problem of broad F-to-J_{CN} mapping, however, is generic for the light nuclei.

VI. SUMMARY AND CONCLUSION

The present work describes an experimental measurement of the evaporation-residue-gated high-energy γ-ray spectra in the reaction $^{19}F + ^{27}Al$ at two beam energies of ∼75 and 125 MeV. Measurements were made in coincidence with a low-energy γ-ray multiplicity detector array in order to address the angular-momentum dependence. The compound nuclear angular momenta populated at the higher beam energy should extend beyond the critical value for the Jacobi shape transition, whereas those at the lower beam energy are expected to be mostly restricted below this value. Although the evidence of such a shape transition is seen in earlier works, the present paper describes a systematic evaporation-residue-gated measurement, addressing the shape transition over a wide range of angular momenta. Particularly, the present work addresses the issue of both the occurrence of this transition at high J and its absence at low J. From the statistical model analysis of the measured spectra for different fold windows (fold is defined earlier and is related to angular momentum), the inverse photoabsorption cross sections were derived at both beam energies. The essential results related to these cross sections can be summarized as follows. At the higher beam energy, a narrow low-energy component is seen which becomes prominent at higher folds. Also, a broad high-energy component is consistent with the data. These observations imply the occurrence of the Jacobi transition at a high angular momentum. Although at the lower beam energy a narrow low-energy component is also witnessed at the lower folds, it is less prominent. Moreover, the data at the higher folds do not show this component. This, therefore, should have a different origin and cannot be related to the angular-momentum-driven effect. The comparison of the data at two beam energies indicates that the critical angular momentum for the Jacobi transition is consistent with the theoretical prediction of $\sim 28\hbar$. Because of the broad mapping of fold to angular momentum, which is generic for any light system, a precise experimental value for this critical angular momentum is somewhat difficult to ascertain. The situation should be better in heavy nuclei, for which this mapping should be narrower.

ACKNOWLEDGMENTS

The authors thank R Kujur, S. Behera, and M. Pose for their help during the experiment, and the accelerator staff at the PLF Mumbai for the smooth operation of the machine.

[1] S. Cohen, F. Plasil, and W. J. Swiatecki, Ann. Phys. (NY) **82**, 557 (1974).
[2] W. D. Myers and W. J. Swiatecki, Acta Phys. Pol. B **32**, 1033 (2001).
[3] M. Kicinska-Habior, K. A. Snover, J. A. Behr, C. A. Gossett, Y. Alhassid, and N. Whelan, Phys. Lett. B **308**, 225 (1993).
[4] A. Maj *et al.*, Nucl. Phys. A **731**, 319 (2004).
[5] Deepak Pandit *et al.*, Phys. Rev. C **81**, 061302(R) (2010).
[6] D. R. Chakrabarty, V. M. Datar, Suresh Kumar, E. T. Mirgule, A. Mitra, V. Nanal, and H. H. Oza, Phys. Rev. C **69**, 021602(R) (2004).

[7] GEANST version 3.21, CERN program library.
[8] D. R. Chakrabarty, V. M. Datar, Suresh Kumar, E. T. Mirgule, A. Mitra, V. Nanal, R. G. Pillay, and P. C. Rout, J. Phys. G **37**, 055105 (2010).
[9] F. Puhlhofer, Nucl. Phys. A **280**, 267 (1980).
[10] W. Nelson, H. Hirayama, and D. Roger, Stanford University Report SLAC-265, 1985 (unpublished).
[11] A. V. Ignatyuk, G. N. Smirenkin, and A. S. Tishin, Sov. J. Phys. **21**, 255 (1975).
[12] M. Brekiesz *et al*., Nucl. Phys. A **788**, 224c (2007).
[13] M. C. Mermaz, J. Barrette, and H. E. Wegner, Phys. Rev. C **24**, 2148 (1981).
[14] R. E. Pywell and M. N. Thompson, Nucl. Phys. A **318**, 461 (1979).
[15] S. M. Dietrich and B. L. Berman, At. Data Nucl. Data Tables **38**, 199 (1988).
[16] D. R. Chakrabarty, Nucl. Instrum. Methods A **560**, 546 (2006).
[17] G. Rusev *et al*., Phys. Rev. C **77**, 064321 (2008), and references therein.